


Tissue-engineered human embryonic stem cell-containing cardiac patches: evaluating recellularization of decellularized matrix

Camila Hochman-Mendez^{1,2}, Dilza Balteiro Pereira de Campos^{1,2},
Rafael Serafim Pinto¹, Bernardo Jorge da Silva Mendes¹,
Gustavo Miranda Rocha¹, Gustavo Monnerat¹,
Gilberto Weissmuller¹, Luiz C Sampaio²,
Adriana Bastos Carvalho^{1,3}, Doris A Taylor² 
and Antonio Carlos Campos de Carvalho^{1,3}

Abstract

Decellularized cardiac extracellular matrix scaffolds with preserved composition and architecture can be used in tissue engineering to reproduce the complex cardiac extracellular matrix. However, evaluating the extent of cardiomyocyte repopulation of decellularized cardiac extracellular matrix scaffolds after recellularization attempts is challenging. Here, we describe a unique combination of biochemical, biomechanical, histological, and physiological parameters for quantifying recellularization efficiency of tissue-engineered cardiac patches compared with native cardiac tissue. Human embryonic stem cell-derived cardiomyocytes were seeded into rat heart atrial and ventricular decellularized cardiac extracellular matrix patches. Confocal and atomic force microscopy showed cell integration within the extracellular matrix basement membrane that was accompanied by restoration of native cardiac tissue passive mechanical properties. Multi-electrode array and immunostaining (connexin 43) were used to determine synchronous field potentials with electrical coupling. Myoglobin content (~60%) and sarcomere length measurement (>45% vs 2D culture) were used to evaluate cardiomyocyte maturation of integrated cells. The combination of these techniques allowed us to demonstrate that as cellularization efficiency improves, cardiomyocytes mature and synchronize electrical activity, and tissue mechanical/biochemical properties improve toward those of native tissue.

Keywords

Decellularized extracellular matrix, cardiomyocytes, recellularization efficiency, mechanical properties

Received: 28 October 2019; accepted: 27 March 2020

Introduction

The extracellular matrix (ECM) is a dynamic framework composed of functional and structural molecules that affect a wide variety of cellular activities. These molecules, which are secreted by resident cells, are arranged in a unique, tissue- and region-specific manner that is suited to the local physiology. Their composition and structure are continuously modified in response to the metabolic activity of resident cells, the mechanical demands of the tissue, and conditions prevailing in the microenvironment. The ECM, in turn, affects cell function and fate. This

¹Instituto de Biofísica Carlos Chagas Filho, Universidade Federal do Rio de Janeiro, Rio de Janeiro, Brazil

²Regenerative Medicine Research, Texas Heart Institute, Houston, TX, USA

³National Institute of Science and Technology for Regenerative Medicine, Universidade Federal do Rio de Janeiro, Rio de Janeiro, Brazil

Corresponding authors:

Doris A Taylor, Regenerative Medicine Research, Texas Heart Institute, 6770 Bertner Avenue, MC 1-135, Houston, TX 77030, USA.
Email: dtaylor@texasheart.org

Antonio Carlos Campos de Carvalho, Instituto de Biofísica Carlos Chagas Filho, Universidade Federal do Rio de Janeiro, Av. Carlos Chagas Filho 373, Rio de Janeiro, 21941-902, Brazil.
Email: acarlos@biof.ufrj.br



“dynamic reciprocity” between the ECM and resident cell population¹ is the one significant advantage over synthetic scaffolds for tissue engineering. Therefore, it is important to keep the native ECM composition intact as maximumly possible, during the preparation of three-dimensional (3D) supports. Doing so provides a microenvironment that promotes cell incorporation and maturation.^{2,3}

Acellular ECM can be generated from cadaveric heart through a process called decellularization,⁴ which involves efficiently removing cytoplasmic and nuclear material while, ideally, minimizing any adverse effects on the composition, biological activity, or mechanical integrity of the remaining ECM. Multiple methods can be used to assess whether these essential properties have been retained after cardiac decellularization. Gross pathologic analysis of cardiac ECM can show whether the cardiac macrostructure was preserved,⁵ whereas high-resolution imaging can be used to examine the preservation at the micro- and nanoscale.⁶ Furthermore, proteomic analysis of decellularized ECM (dECM) can show whether critical structural proteins, such as fibrillin-1, collagen IV, collagen VI, and laminin, were preserved after cell removal with sodium dodecyl sulfate (SDS).^{6,7} Such findings would suggest that the dECM retained the architecture and composition of the native tissue,^{8,9} forming an acellular scaffold that could potentially be recellularized.

Despite improvements in recellularization methods,¹⁰ validating recellularization efficiency is a major challenge. The main goal of the current work was to identify parameters for assessing recellularization efficiency to reveal and quantify recellularization efficiency by demonstrating native-like electrical and mechanical properties, and in doing so, obtaining cardiac tissue with physiological responses. We had five main findings: (1) human embryonic stem cell-derived cardiomyocytes (hESC-CMs) appropriately integrated into and repopulated rat heart dECM, (2) myoglobin levels increased in recellularized ECM and may serve as a surrogate for recellularization efficiency, (3) integrated hESC-CMs showed electrical coupling as indicated by synchronous depolarization, (4) recellularization restored the elastic properties of the dECM scaffolds, giving them properties similar to those of fresh cadaveric tissue, and (5) the ECM elastic modulus varied with cell type and density and may serve as a surrogate for recellularization efficiency.¹¹

Materials and methods

Animals

Animal experiments were performed according to the *Guide for the Care and Use of Laboratory Animals* (eighth edition) and were approved by the Committee on Animal Research and Ethics (CARE) at the Federal University of Rio de Janeiro (reference number 161/13). We used

Wistar lineage rats (*Rattus norvegicus albinus*) that were 3–4 months old and weighed 200–300 g. They were kept at a controlled temperature (23°C) with a 12-hour light–dark cycle and had access to water and standard chow ad libitum.

Heart extraction and decellularization

To avoid blood clotting, we administered 200 µL of sodium heparin (Hepamax-S, Blau Farmacêutica) intraperitoneally 10 minutes before the rats were euthanized with an overdose of pentobarbital–thiopental (Tiopentax, Cristália). After euthanasia, rat hearts were exposed and removed surgically while maintaining the integrity of the aorta. The heart decellularization technique used was adapted from a protocol previously described by the Taylor group.⁴ Briefly, after each heart was excised, the ascending aorta was attached to a cannula integrated into a Langendorff system. Using a peristaltic pump (Minipuls 3, Gilson) set at 4 mL/min, we perfused the heart with phosphate-buffered saline (PBS) for 15 minutes to remove blood from the organ. Then, we perfused the heart with two detergents: SDS (Sigma-Aldrich), an anionic surfactant, was initially perfused at a concentration of 1% v/v for 12 hours, and then Triton X-100 (Sigma-Aldrich), a non-ionic surfactant, was perfused at a concentration of 1% v/v for 15 minutes. The detergent solutions were removed by perfusing the heart with distilled water for 12 hours at room temperature. Both physical (e.g., elasticity) and structural (e.g., matrix protein content and microscopic organization) parameters of the dECM scaffolds were subsequently analyzed.

Decellularization quality control monitoring

Decellularization perfusate turbidity. The decellularization process was monitored by quantifying the turbidity in the outflow of the bioreactor output during heart perfusion, which correlates with cell removal as previously described.¹⁰ Briefly, perfusate samples from the bioreactor outlet were collected at different time points throughout the decellularization process, and turbidity was measured by spectrophotometry at 280 nm absorbance, in duplicate, using a Tecan Infinite M200 Microplate Reader (Tecan Trading AG, Switzerland). The protein concentration was quantified using the Pierce BCA Protein Assay kit (ThermoFisher Scientific, #23225) as per the manufacturer’s instructions. A 25 µL of sample and standards were loaded into a 96-well plate, followed by the addition of 200 µL working reagent (WR) and 30-minute incubation. The resulting fluorescence was read at 562 nm using a Tecan Infinite M200 Microplate Reader (Tecan Trading AG, Switzerland).

Residual glycosaminoglycan (GAG). Glycosaminoglycan was measured using a Blyscan™ Glycosaminoglycan assay kit

(Blyscan, #B1000). The dECM samples (~10 mg wet weight) were digested in a papain extraction reagent solution (papain solution buffer made of sodium phosphate, sodium acetate, ethylenediaminetetraacetic acid (EDTA) disodium salt, and L-cysteine HCl) at 65°C for 3 hours. The Blyscan Glycosaminoglycan assay kit (Blyscan, #B1000) was used to quantify the remaining sulfated GAG; the dye reagent binds to the sulfated GAG in solution, and the dissociation reagent enhances dye absorption during spectrophotometer readings. The absorbance levels of the samples and standards were read in duplicate using a Tecan Infinite M200 Microplate Reader (Tecan Trading AG, Switzerland) at 656 nm. All sulfated GAG concentrations of decellularized tissue were compared to those in the native heart to obtain the percentage of residual sulfated GAG in dECM hearts.

Residual sodium dodecyl sulfate (SDS). A methylene blue (Alfa Aesar/ThermoFisher Scientific, #A18174) SDS quantification assay,¹² as described previously, was adapted to compare residual SDS in tissue to known concentrations of SDS using existing decellularization techniques. The dECM tissue samples were cut to ~10 mg wet weight. Ultrapure water (200 μ L) was added to each sample, and the tissue was homogenized to release residual SDS into solution. The SDS solution extracted from tissue samples was then mixed with methylene blue solution (12 mg of methylene blue in 0.01 M HCl) and chloroform to allow the methylene blue to ionically bind to residual SDS and settle in the organic layer. The resulting fluorescence was read in duplicate at 562 nm using a Tecan Infinite M200 Microplate Reader (Tecan Trading AG, Switzerland) with absorbance at 655 nm. The amount of residual SDS was calculated based on dry weight of the tissue.

Proteomics

Sample preparation. Briefly, protein samples from heart matrices were precipitated with 10% (1:4 v/v) trichloroacetic acid in acetone (Sigma-Aldrich) followed by centrifugation for 15 minutes at 4°C and 15,000 rpm. The samples were washed three times with cold acetone and air dried. Proteins were suspended in 15 μ L of 7 M urea/2 M thiourea (Sigma-Aldrich) and were quantified using a Qubit Protein Assay Kit (Thermo Scientific). Proteins were reduced with 10 mM dithiothreitol (DTT; Sigma-Aldrich) by incubation for 1 hour at 30°C followed by alkylation by incubation with 55 mM iodoacetamide (IAM; Sigma-Aldrich) for 30 minutes in the dark at room temperature. After alkylation, 50 mM NH₄HCO₃ (10:1 v/v; Sigma-Aldrich) and mass spectrometry (MS)-grade trypsin (Promega) at a ratio of 50:1 (protein: trypsin) were added to the proteins, which were incubated overnight at 35°C. After digestion, the samples were acidified using 0.1% trifluoroacetic acid (TFA; Sigma-Aldrich). Peptides

were cleaned with an in-house-prepared C-18 column and eluted in 50 μ L of 50% acetonitrile (ACN)/0.1% TFA followed by 50 μ L of 70% ACN/0.1% TFA; the peptides were dried in a SpeedVac concentrator (Thermo Scientific) and resuspended in 15 μ L of 0.1% formic acid (Sigma-Aldrich). Then, the peptides were quantified using a Qubit Protein Assay Kit and suspended to a final concentration of 0.25 μ g/ μ L in 0.1% formic acid.

Sample and data analysis. Samples were analyzed in three technical replicates by liquid chromatography tandem MS. Briefly, 4 μ L of the diluted samples were applied to an EASY-nLC 1000 system (Thermo Scientific) coupled online to an nESI-Q-Exactive Plus mass spectrometer (Thermo Scientific). Peptides were loaded into a trap column (EASY-ColumnTM, 2 cm, ID100 μ m, 5 μ m, 120A, C18-A1, Thermo Scientific) and eluted in an analytical column (75 μ m \times 25 cm) packed in-house with ReproSil-Pur 120 C18-AQ, 3 μ m (Dr. Maisch, Ammerbuch, Germany). Peptide separations were performed using a gradient from 95% solution A (0.1% formic acid, 5% acetonitrile) to 5%–20% solution B (0.1% formic acid, 95% acetonitrile; Sigma-Aldrich) over 120 minutes, followed by 20%–40% solution B over 40 minutes, and then a 40%–95% solution B over 7 minutes. The peptides were maintained in 95% solution B for 13 minutes. MS1 spectra were acquired in a positive mode using the data-dependent automatic (DDA). Each DDA consisted of a survey scan in the m/z range of 350–2000 and a resolution of 70,000 (at m/z 200) with an automatic gain control target value of 1×10^{-6} ions. The 20 most intense ions were subjected to MS2 acquisition using higher-energy collisional dissociation (HCD) normalized dissociation of previously selected ions, a resolution of 17,500 and automatic gain control (AGC) of 1×10^{-6} ions. MS data were analyzed with PatternLab (v4.0.0.62) using a Uniprot Rattus norvegicus database downloaded in June 2019. Search parameters were semi-tryptic hydrolysis, two missed cleavages, oxidation of methionine as variable and carbamidomethylation as fixed modifications, and a peptide tolerance of 40 ppm. The validity of the peptide sequence matches was assessed using SEPro v2.2.0.2. A cutoff score was established to accept a false discovery rate of 1% based on the number of decoys. A minimum sequence length of six amino acids was required. The results were postprocessed to accept peptide sequence matches with less than 5 ppm. Proteins were identified according to the maximum parsimony approach as described previously.¹³ Search parameters were for tryptic peptides, two missed cleavages, oxidation of methionine, n-terminal protein acetylation, as variable modification, and carbamidomethylation as static modifications, and a precursor mass tolerance of 10 ppm and fragment mass tolerance of 0.05 Da. A cutoff score was established to accept a false discovery rate of 1%, using Percolator. Proteins were grouped according to the maximum parsimony approach.

Cardiomyocyte differentiation

The human embryonic stem cells (line hES3-Nkx2.5 eGFP)¹⁴ used in this study were kindly donated by Monash University (Victoria, Australia), and the insertion of eGFP on the Nkx-2.5 locus was described in detail by Elliot and colleagues.¹⁴ The hESCs were differentiated to form cardiomyocytes (CMs) in cardiac embryoid bodies. Cardiac differentiation was performed as described by Kattman et al.¹⁵ At 15 days of the differentiation protocol, the cardiac embryoid bodies were dissociated with collagenase II overnight and then incubated with trypsin-EDTA 0.025% for 15 minutes. Differentiation efficiency was evaluated using flow cytometry to assess staining for cardiac troponin T (anti-cardiac troponin T antibody, Thermo Scientific, cat #MA5-12960). Cell preparations were used for further experimentation only if more than 60% of the cells were positive for troponin T (Supplemental Figure 1(a)).

Scaffold recellularization

Whole-heart decellularized scaffolds were immersed in a solution containing amphotericin B, penicillin, and streptomycin in PBS for 3 days. After this treatment, the decellularized scaffolds were washed with PBS and dissected into 1.5 mm² segments of decellularized left atrium (dLA) and decellularized left ventricle (dLV). Atrial and ventricular scaffolds were co-cultured separately for 15 days with 5×10^5 hESC-CMs in a non-adherent plate pretreated with poly 2-hydroxyethyl methacrylate (Sigma-Aldrich, cat #P3932). For the first 2 days of this process, the plates were cultured on an orbital shaker set at 30–50 rpm. Cell retention percentage was calculated after this first 48 hours based on the following equation: retention (%) = (total number of cells seeded – (floating cells + plate-attached cells) / total number of cells seeded) \times 100. The number of non-attached cells (Supplemental Figure 1(b)) was obtained by combining the number of trypan blue⁻ (live) and trypan blue⁺ (dead) cells on both the supernatant (floating cells) and on the plates (plate-attached cells). hESC-CMs cultured as embryoid bodies (on a non-adherent plate) for 15 days without a scaffold were used as a control. All cells and constructs were cultured in StemPro-34 supplemented medium (Thermo Fisher Scientific) at 37°C with 5% CO₂ and 95% air, with medium changes every 2 days.

Immunostaining

Cadaveric (cLV), decellularized (dLV), and recellularized cardiac patches (recellularized left atrium (rLA) and recellularized left ventricle (rLV)) were fixed by incubating them with 2% paraformaldehyde overnight at 4°C with agitation. These samples underwent sequential cryopreservation (10%, 20%, and 30% D-sucrose) and were blocked

in optimal cutting temperature compound and sliced in a cryostat (CM1850—Leica®). For fluorescence imaging, thin sections (10 μm) were washed three times for 5 minutes in PBS and incubated with 5% bovine serum albumin in PBS for 30 minutes. These sections were incubated with a primary antibody (anti-laminin (1:100) Abcam, cat #ab11575; anti-connexin 43 (1:100) Abcam cat #ab87645; or anti-GFP (1:500) Abcam, cat #ab1218) overnight at 4°C, washed three times in PBS (5 minutes each), and then incubated with a secondary antibody (anti-rabbit Alexa Fluor 546 (1:400) Thermo Fisher Scientific, cat #A11010 or anti-mouse Alexa Fluor 488 (1:400) Thermo Fisher Scientific, cat #A11001) for 1 hour at room temperature. Subsequently, the samples were washed three times in PBS (5 minutes each) and once with distilled water before being mounted with a fluorescence signal loss attenuator and stained with DAPI (ProLong® Gold with DAPI, Life Technologies). Confocal images were obtained with a Nikon Intensilight A1 + confocal laser scanning microscope. After recellularization, cellularity was evaluated by quantifying the percentage of tissue area covered by GFP⁺ staining in 20 images of three different heights of four different recellularized patches of both rLA and rLV sectioned and GFP and laminin-stained slides.

Ultrastructural evaluation

Samples of recellularized dECM (rLV and rLA) and cells (hESC-CMs) were fixed in Karnovsky's solution (4% paraformaldehyde and 2.5% glutaraldehyde in 0.1M cacodylate buffer, pH 7.2) for 2 hours and then washed with 0.1M sodium cacodylate buffer (pH 7.2). Subsequently, they were dehydrated using increasing concentrations of ethanol and dried using a Balzers CPD 050 critical point dryer. Finally, the samples were coated with a thin gold layer using a sputter coater (Bal-Tec SCD 050) and visualized with a Jeol 5310 scanning electron microscope.

Tension assessments

An atomic force microscope (BioScope Catalyst, Bruker) was used in “force volume” operating mode to obtain the elastic modulus of cLV, dLV, and rLA and rLV. To prevent samples from moving during data acquisition, they were held in place by a platinum hook attached to the bottom of a 35 mm petri dish. Measurements were acquired with DNP-S Silicon Nitride probes (Bruker). The cantilever elastic constants were obtained using the thermal noise method. The indentation rates were less than 2 μm/s, and most measurements were performed at a rate of 1 Hz with an indentation depth less than 2 μm. Areas without staining (low cell density) and GFP-stained areas (CM) were identified using fluorescence microscopy. Force volume measurement was performed pixel by pixel in five different 250 μm²-areas (generating 256 force curves per spot;

Supplemental Figure 2) of each of these two regions (low cell density and CM). Peakforce measurements were obtained from 120 to 180 random spots in three samples of each condition. Force curves, heights, 3D reconstructions, and depth histograms were analyzed with NanoScope Analysis 1.5 software (Bruker), and the force curves were converted to Young's modulus data.

Cardiomyocyte maturation

Myoglobin quantification. Myoglobin was measured using the Human Myoglobin ELISA Kit (Abcam, cat #ab171580) according to the manufacturer's instructions. In brief, 50 μ L of sample or cadaveric tissue (control) was extracted by using cell extraction buffer PTR and dispensed into the appropriate wells in the presence of the antibody cocktail. The plates were sealed and incubated on a plate shaker (set to 400 rpm) at room temperature for 1 hour. The contents of the wells were removed, and the plates were washed three times with wash buffer PT. After the last wash, any residual liquid was removed by striking the plates sharply onto paper towels. After the wash step, 100 μ L of 3,3',5,5'-tetramethylbenzidine development solution was added to each well, and the plates were incubated in the dark with agitation at room temperature for 10 minutes. The reaction was stopped by adding 100 μ L of stop solution to each well. After a gentle 1-minute mix, the absorbance was read at 450 nm using a plate reader (Tecan Infinite M200 Pro).

Sarcomere length. Cardiomyocyte maturation was evaluated using transmission electron microscopy (TEM) to measure sarcomere length. For TEM, samples were fixed with Karnovsky's solution for 4 hours and then underwent postfixation in 1% osmium tetroxide. After dehydration, samples were mounted in epoxy resin (Araldite Durcupan ACM, Fluka) and sliced in an ultramicrotome to yield 100 nm sections. The ultra-thin slices were deposited on copper grids and stained with 2% uranyl acetate and lead citrate. TEM images were acquired with a JEM 1200EX II (Jeol).

Microelectrode array analysis. To evaluate the electrical properties of the recellularized tissues, including the action potential wave propagation, we placed the tissues in a six-well microelectrode array (MEA) chamber on Day 15 of the recellularization protocol (60 and six-well MEA200/30iR/ 30iR-Ti-tcr, Multi-Channel Systems, Germany). To increase the interaction between the recellularized matrices and the MEA electrodes, we placed a glass coverslip (0.13 mm) over the microtissue. With the samples at 37°C, field potentials were acquired after 5 minutes at a sample rate of 10 kHz with Cardio 2D. The cellular electrical activity in four non-adjacent electrodes was analyzed with Cardio 2D+.

Statistical analysis

Data are shown as mean \pm standard deviation. The nucleic acid content of the cadaveric and dECM groups was compared using the Student *t* test. All other data (myoglobin content, sarcomere length, and elastic modulus) were analyzed using one-way analysis of variance with Tukey's multiple comparisons test. A *p*-value < 0.05 was considered significant. GraphPad Prism[®] software version 7.0 (GraphPad Software, Inc.) was used for all statistical analyses.

Results

Preserved ECM characteristics promoted adherence of hESC-CMs and synchronous macroscopic contractions of the cardiac patches

Rat hearts were decellularized using a technique previously described by our group,⁴ as shown in the timeline (Figure 1(a)). Decreased turbidity after SDS treatment (Figure 1(b)) yielded translucent, cell-free dECM scaffolds with low DNA content (51.3 ± 23.9 ng/mg, reduced approximately 12-fold compared with cadaveric tissue) and SDS (0.04 ± 0.019 μ g/mg) levels, and preserved GAG (2.56 ± 0.53 μ g/mg) content (Figure 1(c)). Using a matrixome database,¹⁶ we identified 23 proteins from the core matrixome—mainly collagens and ECM glycoproteins—and 9 proteins from matrixome-associated proteins, including ECM-affiliated proteins, ECM regulators, and secreted factors (Figure 1(d)). All identified proteins are listed in Supplemental Table 1. Therefore, the micro-architecture of the dECM was highly preserved (Figure 1(e)), including the wave-like pattern of the basement membrane laminin that follows the Z-disk structures in cardiomyocyte sarcolemma (Figure 1(d) insert).

Myoglobin content was present in recellularized ECM but could not be detected in dECM

The dECM scaffolds were dissected to generate dLA- or dLV-derived patches. Isolated dLA and dLV were recellularized with hESC-CMs expressing green fluorescent protein (GFP) under the control of the Nkx-2.5 gene promoter region. To accomplish this, we used an agitation-based process, as described in the "Methods" section, to seed the hESC-CMs onto pieces of dLA and dLV (retention rate of $\sim 80\%$, Figure 2(a)) and then co-cultured the ECM pieces and cells for 15 days in vitro. This recellularization method produced beating of both the rLA and rLV (Supplemental Movie 1). When compared visually with their decellularized counterparts, the rLA and rLV were darker in color (Figure 2(b)), suggesting the presence of proteins containing a heme group, such as myoglobin, a protein present in

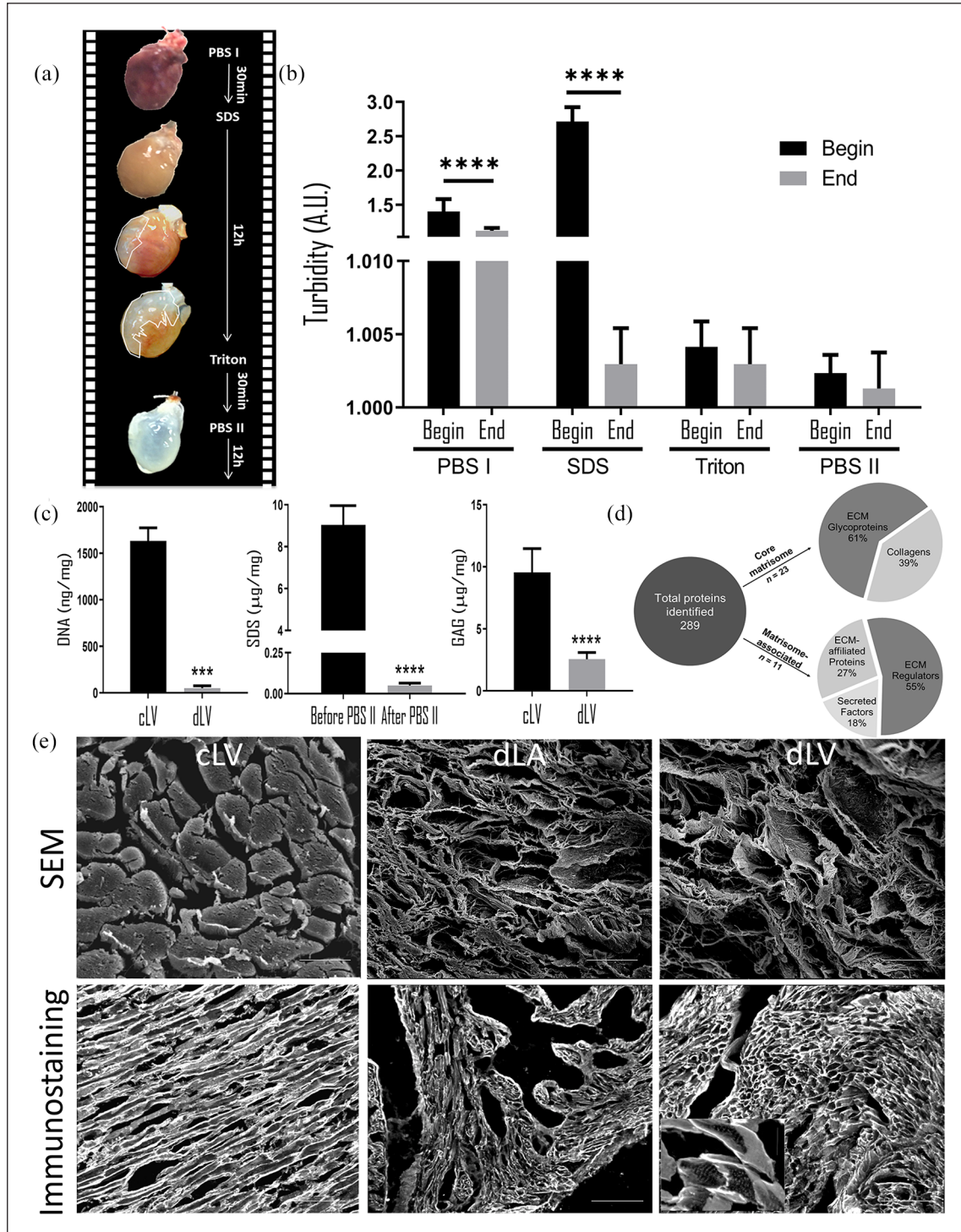


Figure 1. Decellularization and characterization of rat hearts: (a) Timeline and time-lapse images of the rat heart through the first 25 hours of the decellularization process. (b) Cellular debris removal calculated as the mean value of turbidity ($n = 15$ hearts) at the beginning (black bars) and end of the decellularization process (gray bars). Data are mean \pm s.d. (c) Remaining SDS, GAG, and DNA in cadaveric ($n = 6$) and decellularized ($n = 8$) hearts. Data are mean \pm s.d. (d) Proteomic analysis of dLV ($n = 2$). (e) Laminin immunostaining and scanning electron microscope images of cLV, dLA, and dLV. Scale bars: 100 μm (upper panels) and 200 μm (lower panels).

The insert shows high magnification of dLV. Scale bar: 10 μm . $***p < 0.0001$. Two-way ANOVA with multiple comparisons was used for statistical analysis. cLV: non-decellularized left ventricle, dLA: decellularized left atrium, dLV: decellularized left ventricle.

muscle cells. To determine whether myoglobin was present and whether the myoglobin level in recellularized ECM could serve as a surrogate marker of recellularization, we compared the myoglobin level in rLA and rLV with that in human cLV, dLA and dLV, and an equal number of hESC-CMs cultured without a scaffold (Figure 2(c); $n=4$ per group). Myoglobin could not be detected in the dLA or dLV (i.e., it was below the detection limit of the kit), whereas the myoglobin levels in the rLA and rLV were approximately 57% and 55%, respectively, of the level in cadaveric heart tissue; this represented a four- to fivefold increase in myoglobin level in both the rLA ($0.260\text{ mM} \pm 0.009$) and rLV ($0.249\text{ mM} \pm 0.001$) compared with the level in hESC-CMs cultured alone ($0.077\text{ mM} \pm 0.017$) (Figure 2(c)).

hESC-CMs appropriately integrated into and repopulated rat heart dECM showing electrical coupling as indicated by synchronous depolarization

To evaluate cell adhesion and integration, we fixed the rLA and rLV tissues, sliced the tissues transversely (Figure 2(d)), and immunostained them to show the hESC-CMs (GFP staining) and ECM (laminin staining). As anticipated by the contractile activity (Supplemental Movie 1), CMs were present in both the rLA and rLV. On general observation, we identified areas with a high density of CMs (squares) and with a low cardiomyocyte density (circles). High-magnification images of the areas with high cardiomyocyte density in both rLA and rLV further indicated that the CMs were surrounded by ECM (Figure 2(d)). Quantification of the recellularized areas revealed that the rLA comprised $47.97\% \pm 14.36\%$ of GFP⁺ cells and the rLV comprised $41.29\% \pm 13.65\%$ (Figure 2(e)). In TEM images, the organization of the contractile apparatus was evident in the rLA and rLV. Cardiomyocyte sarcomere length was greater in both rLA ($1.622 \pm 0.301\ \mu\text{m}$; $n=10$) and rLV ($1.734 \pm 0.313\ \mu\text{m}$; $n=9$) than in the cultured hESC-CMs ($1.165 \pm 0.177\ \mu\text{m}$; $n=8$) (Figure 2(f)).

To evaluate the electrical coupling within the rLA and rLV patches, we analyzed the tissues via MEA (Figure 3(a)). Both tissue groups showed synchronous depolarization in non-adjacent regions, and immunostaining revealed that connexin 43 (Cx43) was present in intercalated disk-like structures (Figure 3(b)) at the edge of the cells.

Recellularization restored the elastic properties of the dECM scaffolds similar to that in cadaveric tissues

In our in-depth evaluation of rLA and rLV, we identified areas with low cell density, in addition to the high cell density areas already described. Using atomic force

microscopy (AFM) combined with fluorescence microscopy, we measured the elastic modulus, a measure of distensibility, in the two distinct areas: (1) low cell density areas and (2) areas with cardiomyocytes (CMs) (Figure 4(a)). Data obtained from these three areas were compared to elastic moduli obtained from dLV and cLV. We demonstrated that decellularization decreased the elastic modulus of heart tissue (cLV: $10.689 \pm 1.345\text{ kPa}$ vs dLV: $1.913 \pm 0.701\text{ kPa}$, Figure 4(b)). After the dECM was recellularized, we observed an interesting phenomenon. At the edges of the low cell density areas, where few or no cells were present, the elastic modulus (dLA: $2.801 \pm 0.619\text{ kPa}$ and dLV: $3.005 \pm 0.897\text{ kPa}$; Figure 4(b)) was similar to that of decellularized tissue. However, the elastic modulus of the areas with CMs (rLA: $10.488 \pm 0.966\text{ kPa}$ and rLV: $10.495 \pm 1.125\text{ kPa}$; Figure 4(b)) was similar to that of cadaveric tissue.

Discussion

The goal of this study was to establish parameters for evaluating recellularization efficiency in cardiac patches made with CMs derived from human pluripotent stem cells (PSCs). We used rat heart ECM as a scaffold source because the free wall of the left ventricle generated constructs small enough to be recellularized with obtainable numbers of human CMs that could still be measured as a whole in the atomic force microscopy after recellularization. Although this configuration can be used preclinically to evaluate the safety and efficacy of constructs populated with hESC-CMs, rat ECM scaffolds are not adequate for use in humans. Thus, our ongoing studies are aimed at using human-sized scaffolds and scaling up the production of human induced PSC-derived cardiac cells,¹⁷ including CMs, to the numbers required to engineer human-sized cardiac tissues and hearts in vitro.

Here, the preserved ECM characteristics promoted adherence of CMs to the scaffolds and synchronous macroscopic contractions of the cardiac patches. To our knowledge, this is the first time that cells have been shown to incorporate into the basement membrane of the dECM (as would be required for successful bioengineering of native-like cardiac tissue) rather than being confined to the point of cell injection.⁴ Also, the CMs engrafted into the dECM and displayed synchronous action potentials, as detected by MEA, which was supported by the presence of connexin 43 at cell junction areas, as would be expected in functional gap junctions. This finding supports previous data showing electrical coupling of CMs that were cultured on the surface of dECM.^{18,19}

Because hESC-CMs typically have an immature phenotype in vitro,^{20,21} some investigators have seeded these cells on dECM and other biomaterials to induce maturation.^{22–24} We reasoned that incorporation of the cells into the matrix would be superior to surface coating because of

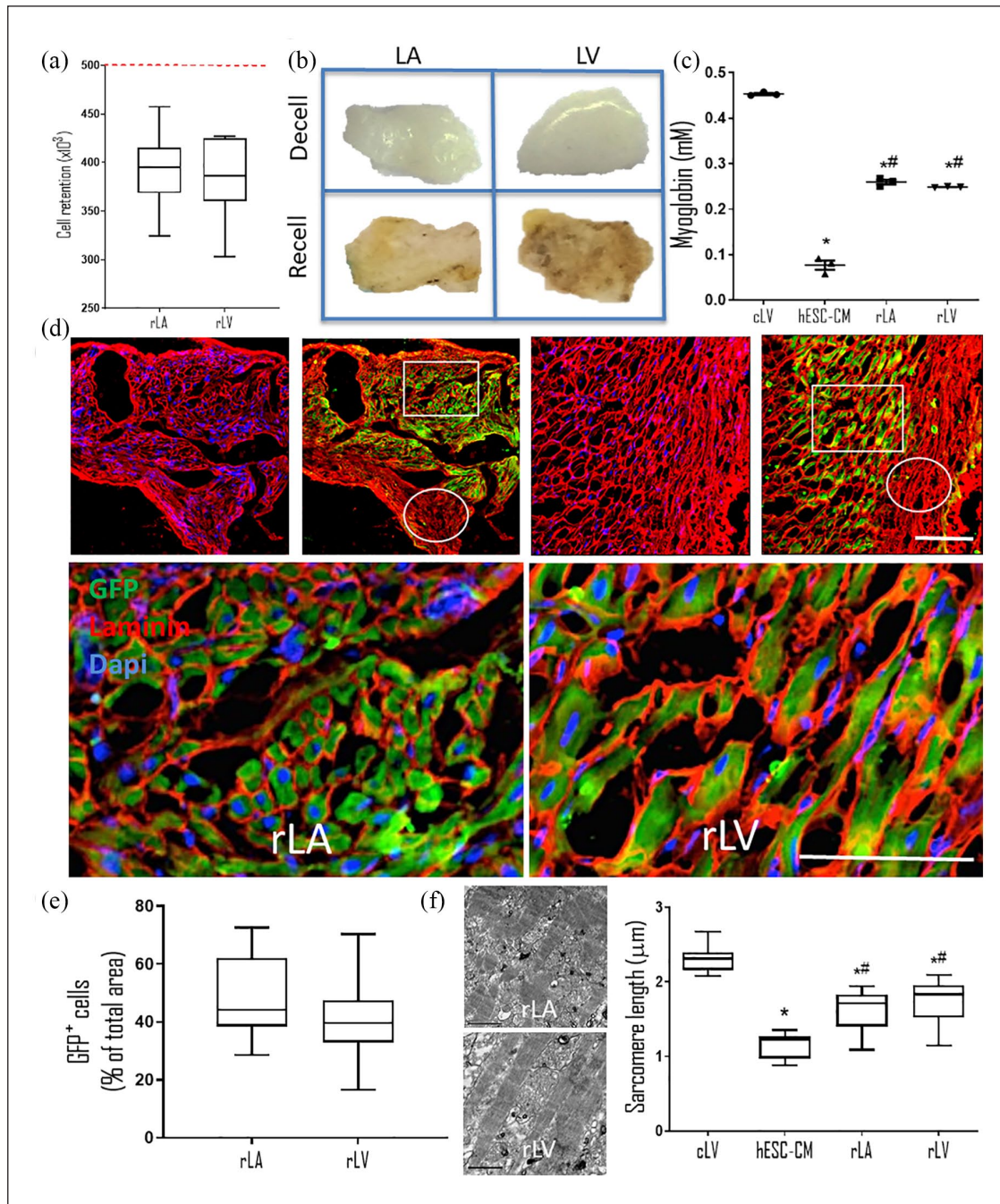


Figure 2. Characterization of CMs retained in recellularized cardiac patches at 15 days: (a) Box plot of cells retained in the rLA and rLV after hESC-derived cardiomyocyte delivery ($n = 10$). Dashed red line represents the number of cells delivered. Data are mean \pm s.d. (b) LA and LV patches before (upper panels) and after (lower panels) recellularization. (c) Myoglobin content of non-decellularized left ventricle (cLV), hESC-CMs, rLA, and rLV. * $p < 0.0001$ versus cadaveric, $p < 0.0001$ versus hESC-CMs. (d) Representative images of transverse sections of rLA and rLV immunostained for GFP (green), laminin (red), and nuclei (blue). Scale bar, 50 μm . (e) Quantification of cellularity after recellularization. Data are shown as mean \pm s.d. (f) Representative transmission electron microscopy images of rLA and rLV. Boxplot showing sarcomere length quantification in cLV, hESC-CMs, rLA, and rLV. * $p < 0.0001$ versus cadaveric, $p < 0.0001$ versus hESC-CMs.

the greater probability of matrix–cell interactions. When the cells are surrounded by cardiac basement membrane, the dynamic reciprocity between the cells and the ECM

provides biochemical and mechanical cues to induce cardiomyocyte maturation. As expected, we found that after only 15 days of culture in the dECM, the sarcomere length

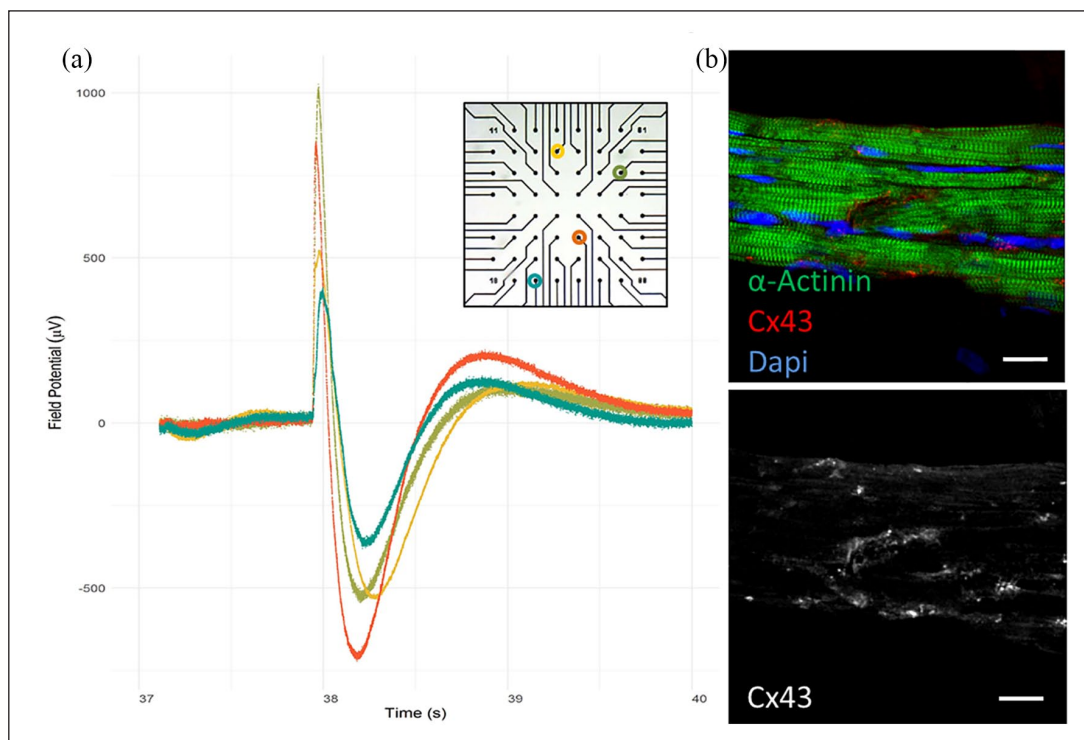


Figure 3. hESC-CMs in recellularized patches exhibited electrical coupling and gap junctions: (a) Overlap of four field potential recordings obtained from different MEA electrodes. Each colored line represents an individual recording from the corresponding electrode in the same color in the inset. (b) Representative images of transverse sections of recellularized dECM immunostained for α -actinin (green), connexin-43 (Cx43; red on the top; white on the bottom), and nuclei (blue). Scale bar: 2 μ m.

of the CMs increased about 40% to 1.6 μ m, which is at the upper range of the sarcomere size in human fetal cardiac myocytes (1–1.7 μ m).^{25–28} Li et al.¹⁹ also showed an increase in sarcomere length when PSC-derived CMs were cultured over dECM, although their reported values (1–2.5 μ m) were above the physiologic range for human CMs in vivo, suggesting overstretch of the cells in their studies.

Functional maturation was also supported by the amount of myoglobin expressed after recellularization. Myoglobin is a cytosolic, oxygen-binding protein responsible for the storage and diffusion of oxygen within myocytes and has been shown to be associated with cardiomyocyte differentiation in vitro.²⁹ Because myoglobin is involved in the lipid metabolism governing fatty acid rather than glucose use,³⁰ its presence in the recellularized dECM suggests that the metabolic activity of the integrated CMs is more like that of normal healthy myocardium (i.e., fatty acids are used more often as an energy source) than that of stem cells. To our knowledge, this study is the first to show that the myoglobin content in human stem cell-derived CMs increases after the cells are cultivated in ECM.

The cardiac ECM affects the heart's passive mechanical properties, such as elasticity,³¹ which contribute

critically to the proper functioning of the heart. Although uniaxial tensile tests have traditionally been used to characterize the mechanical properties of decellularized tissue, AFM and other non-destructive techniques have emerged as alternative approaches to performing nanoindentation tests.³² We analyzed the elastic (Young's) modulus of our constructs with AFM and fluorescence microscopy. Two different and complementary AFM-based modes were used: force volume and PeakForce Tapping[®] (Bruker) modes.

Although absolute values of stiffness vary widely depending on the technique and the region of the heart used to obtain the data,^{11,33} our stiffness values (7–13 kPa) were similar to those previously described for decellularized cadaveric rat heart samples.³⁴ Furthermore, similar to previous reports,³⁵ we found that decellularized matrix (dLV) had a decreased Young's (elastic) modulus as compared to that in cadaveric native hearts (cLV). In contrast, other researchers have reported increased stiffness after decellularization. Disparities in these data are mainly related to different physiological and chemical characteristics of xeno-derived scaffolds³⁶ and to decellularization protocols that result in incomplete cellular DNA removal³⁷ or that leave behind significant cell residue.³⁵

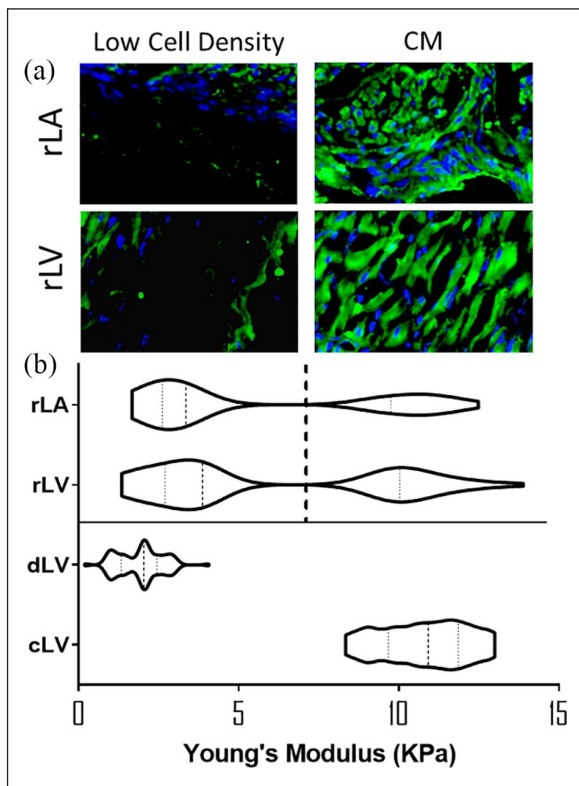


Figure 4. The presence of cardiac cells restores scaffold elasticity toward that of cadaveric heart: (a) Representative images of transverse sections of rLA and rLV immunostained for GFP (green) and nuclei (blue). Scale bar: 50 μ m. Images were obtained from two different regions in rLA and rLV patches: areas with low cell density (few nuclei) and areas with CMs (high amount of GFP⁺ cells). (b) Young's modulus quantification by atomic force microscopy of low cell density and with CM areas of rLA, rLV, dLV, and non-decellularized left ventricle (cLV).

Given the key role of myocardium micro-elasticity in the ejection fraction, restoring the elastic properties is fundamental to reestablishing the function of the ventricle in tissue-engineered products. To this end, we found that recellularized scaffolds showed an increase in the mean elastic modulus. Figure 4 illustrates a bimodal pattern in the elastic moduli of areas within the same patches; the elastic modulus in areas of low cardiomyocyte density was similar to that of decellularized tissue in the areas without cells (absence of nuclei), and the cardiomyocyte-rich regions had an elastic modulus similar to that of cadaveric heart.

These findings suggest that elastic modulus, in addition to myoglobin content, can be used as a measure of recellularization efficiency. Moreover, the increased elastic modulus of the recellularized dECM suggests that patching damaged hearts with recellularized scaffolds *in vivo* could lead to improvements in the passive mechanical properties of the myocardium and, possibly, in diastolic function, eliminating diastolic creep.³⁸

Conclusion

In conclusion, our findings suggest that hESC-CMs can efficiently engraft within the basement membrane of dECM improving elasticity and allowing for synchronized contractions. Our results also suggest that cultivating hESC-CMs in the presence of rat heart dECM improved the physiological maturation of the cells, illustrating expected dynamic reciprocity between the cells and the matrix, despite the latter's xenogeneic source.

Acknowledgments

These authors thank all the members of the Cellular and Molecular Laboratory (LCCM/UFRJ) for their valuable suggestions regarding the experimental design and data interpretation and Texas Heart Institute's Scientific Publications department for editorial assistance.

Authorship

C.H.M., B.J.D.S.M., A.B.C., and A.C.C.D.C. conceived and designed the work. C.H.M., D.B.P.D.C., R.S.P., G.M.R., G.M., and G.W. performed the experiments. C.H.M., D.B.P.D.C., G.M.R., G.M., and G.W. analyzed the data. C.H.M., G.W., A.B.C., and A.C.C.D.C. contributed reagents/materials/analysis tools. C.H.M., D.B.P.D.C., R.S.P., G.M.R., G.W., L.C.S., A.B.C., D.A.T., and A.C.C.D.C. visualized the data. C.H.M., D.B.P.D.C., A.B.C., D.A.T., and A.C.C.D.C. wrote the original article. C.H.M., D.B.P.D.C., G.M.R., G.W., L.C.S., A.B.C., D.A.T., and A.C.C.D.C. reviewed and edited the article.

Data availability statement

The authors declare that the data supporting the findings of this study are available within the article and its supplemental information files. The reader may contact the corresponding authors with any request (dtaylor@texasheart.org; acarlos@biof.ufrj.br).

Declaration of conflicting interests

The author(s) declared the following potential conflicts of interest with respect to the research, authorship, and/or publication of this article: Dr. Doris Taylor has financial interest in Miromatrix Medical, Inc. This relationship is monitored in accordance with the conflict of interest policies by the University of Minnesota and the Texas Heart Institute. The other authors have no conflict of interest to disclose.

Funding

The author(s) disclosed receipt of the following financial support for the research, authorship, and/or publication of this article: This work was supported by grants from the Conselho Nacional de Desenvolvimento Científico e Tecnológico (CNPq; 302864/2017-2); Fundação de Amparo à Pesquisa do Estado do Rio de Janeiro (FAPERJ; 232929; 232323; 205031 and 210459); and Institutos Nacionais de Ciência e Tecnologia (INCT; 465656/2014-7) Brazil.

ORCID iD

Doris A Taylor  <https://orcid.org/0000-0003-0032-1915>

Supplemental material

Supplemental material for this article is available online.

References

- Bissell MJ and Aggeler J. Dynamic reciprocity: how do extracellular matrix and hormones direct gene expression. *Prog Clin Biol Res* 1987; 249: 251–262.
- Badyalak SF, Taylor D and Uygun K. Whole-organ tissue engineering: decellularization and recellularization of three-dimensional matrix scaffolds. *Annu Rev Biomed Eng* 2011; 13: 27–53.
- He M and Callanan A. Comparison of methods for whole-organ decellularization in tissue engineering of bioartificial organs. *Tissue Eng Part B Rev* 2013; 19(3): 194–208.
- Ott HC, Matthiesen TS, Goh SK, et al. Perfusion-decellularized matrix: using nature's platform to engineer a bioartificial heart. *Nat Med* 2008; 14(2): 213–221.
- Sanchez PL, Fernandez-Santos ME, Costanza S, et al. Acellular human heart matrix: a critical step toward whole heart grafts. *Biomaterials* 2015; 61: 279–289.
- Mayorca-Guiliani AE, Madsen CD, Cox TR, et al. ISDoT: in situ decellularization of tissues for high-resolution imaging and proteomic analysis of native extracellular matrix. *Nat Med* 2017; 23(7): 890–898.
- Guyette JP, Charest JM, Mills RW, et al. Bioengineering human myocardium on native extracellular matrix. *Circ Res* 2016; 118(1): 56–72.
- Arenas-Herrera JE, Ko IK, Atala A, et al. Decellularization for whole organ bioengineering. *Biomed Mater* 2013; 8(1): 014106.
- Witzenburg C, Raghupathy R, Kren SM, et al. Mechanical changes in the rat right ventricle with decellularization. *J Biomech* 2012; 45(5): 842–849.
- Lee PF, Chau E, Cabello R, et al. Inverted orientation improves decellularization of whole porcine hearts. *Acta Biomaterialia* 2017; 49: 181–191.
- Engler AJ, Carag-Krieger C, Johnson CP, et al. Embryonic cardiomyocytes beat best on a matrix with heart-like elasticity: scar-like rigidity inhibits beating. *J Cell Sci* 2008; 121(Pt. 22): 3794–3802; 3794–3802.
- Taylor DA, Sampaio LC, Cabello R, et al. Decellularization of whole human heart inside a pressurized pouch in an inverted orientation. *J Vis Exp* 2018(141): e58123.
- Silva Dos Santos D, Brasil GV, Ramos IPR, et al. Embryonic stem cell-derived cardiomyocytes for the treatment of doxorubicin-induced cardiomyopathy. *Stem Cell Res Ther* 2018; 9(1): 30.
- Elliott DA, Braam SR, Koutsis K, et al. NKX2-5(eGFP/w) hESCs for isolation of human cardiac progenitors and cardiomyocytes. *Nat Methods* 2011; 8(12): 1037–1040.
- Kattman SJ, Witty AD, Gagliardi M, et al. Stage-specific optimization of activin/nodal and BMP signaling promotes cardiac differentiation of mouse and human pluripotent stem cell lines. *Cell Stem Cell* 2011; 8(2): 228–240.
- Naba A, Clauser KR, Ding H, et al. The extracellular matrix: tools and insights for the “omics” era. *Matrix Biol* 2016; 49: 10–24.
- Paccola Mesquita FC, Hochman-Mendez C, Morrissey J, et al. Laminin as a potent substrate for large-scale expansion of human induced pluripotent stem cells in a closed cell expansion system. *Stem Cells Int* 2019; 2019: 9704945.
- Garreta E, de Onate L, Fernandez-Santos ME, et al. Myocardial commitment from human pluripotent stem cells: rapid production of human heart grafts. *Biomaterials* 2016; 98: 64–78.
- Li B, Yang H, Wang X, et al. Engineering human ventricular heart muscles based on a highly efficient system for purification of human pluripotent stem cell-derived ventricular cardiomyocytes. *Stem Cell Res Ther* 2017; 8(1): 202.
- Blazeski A, Zhu R, Hunter DW, et al. Electrophysiological and contractile function of cardiomyocytes derived from human embryonic stem cells. *Prog Biophys Mol Biol* 2012; 110(2–3): 178–195.
- Yang X, Pabon L and Murry CE. Engineering adolescence: maturation of human pluripotent stem cell-derived cardiomyocytes. *Circ Res* 2014; 114(3): 511–523.
- Fong AH, Romero-Lopez M, Heylman CM, et al. Three-dimensional adult cardiac extracellular matrix promotes maturation of human induced pluripotent stem cell-derived cardiomyocytes. *Tissue Eng Part A* 2016; 22(15–16): 1016–1025.
- Herron TJ, Rocha AM, Campbell KF, et al. Extracellular matrix-mediated maturation of human pluripotent stem cell-derived cardiac monolayer structure and electrophysiological function. *Circ Arrhythm Electrophysiol* 2016; 9(4): e003638.
- Ogasawara T, Okano S, Ichimura H, et al. Impact of extracellular matrix on engraftment and maturation of pluripotent stem cell-derived cardiomyocytes in a rat myocardial infarct model. *Sci Rep* 2017; 7(1): 8630.
- Guccione JM, O'Dell WG, McCulloch AD, et al. Anterior and posterior left ventricular sarcomere lengths behave similarly during ejection. *Am J Physiol* 1997; 272(1 Pt 2): H469–H477.
- Hanft LM, Korte FS and McDonald KS. Cardiac function and modulation of sarcomeric function by length. *Cardiovasc Res* 2008; 77(4): 627–636.
- Lundy SD, Zhu WZ, Regnier M, et al. Structural and functional maturation of cardiomyocytes derived from human pluripotent stem cells. *Stem Cell Develop* 2013; 22(14): 1991–2002.
- Pollack GH and Huntsman LL. Sarcomere length-active force relations in living mammalian cardiac muscle. *Am J Physiol* 1974; 227(2): 383–389.
- Xu C, Police S, Rao N, et al. Characterization and enrichment of cardiomyocytes derived from human embryonic stem cells. *Circ Res* 2002; 91(6): 501–508.
- Hendgen-Cotta UB, Esfeld S, Coman C, et al. A novel physiological role for cardiac myoglobin in lipid metabolism. *Sci Rep* 2017; 7: 43219.
- Chung CS and Granzier HL. Contribution of titin and extracellular matrix to passive pressure and measurement of sarcomere length in the mouse left ventricle. *J Mol Cell Cardiol* 2011; 50(4): 731–739.
- Tang G, Galluzzi M, Biswas CS, et al. Investigation of micromechanical properties of hard sphere filled composite hydrogels by atomic force microscopy and finite

- element simulations. *J Mech Behav Biomed Mater* 2018; 78: 496–504.
33. Engler AJ, Rehfeldt F, Sen S, et al. Microtissue elasticity: measurements by atomic force microscopy and its influence on cell differentiation. *Methods Cell Biol* 2007; 83: 521–545.
 34. Berry MF, Engler AJ, Woo YJ, et al. Mesenchymal stem cell injection after myocardial infarction improves myocardial compliance. *Am J Physiol Heart Circ Physiol* 2006; 290(6): H2196–H2203.
 35. Merna N, Robertson C, La A, et al. Optical imaging predicts mechanical properties during decellularization of cardiac tissue. *Tissue Eng Part C Method* 2013; 19(10): 802–809.
 36. Shah M, Kc P, Copeland KM, et al. A thin layer of decellularized porcine myocardium for cell delivery. *Sci Rep* 2018; 8(1): 16206.
 37. Methe K, Backdahl H, Johansson BR, et al. An alternative approach to decellularize whole porcine heart. *Biores Open Access* 2014; 3(6): 327–338.
 38. Atkins BZ, Hueman MT, Meuchel J, et al. Cellular cardiomyoplasty improves diastolic properties of injured heart. *J Surg Res* 1999; 85(2): 234–242.